ADVANCED ROBOTICS, 2017
https://doi.org/10.1080/01691864.2017.1318716

FULL PAPER

Safety verification method for preventing friction blisters during utilization of physical assistant robots

Xuewei Mao[a], Yoji Yamada[a], Yasuhiro Akiyama[a], Shogo Okamoto[a] and Kengo Yoshida[b]

[a]Department of Mechanical Science and Engineering, Graduate School of Engineering, Nagoya University, Nagoya, Japan; [b]Reactor Maintenance and Repair Division, Mihama Nuclear Power Plant, Kansai Electric Power Co., Inc., Mihama, Japan

ABSTRACT

This study is mainly concerned with the potential hazards of interactive friction force on a human–robot contact surface, which may result in various skin traumas, such as friction blisters. In this study, a novel safety verification method is developed for helping physical assistant robot users to avoid this hazardous condition. First, based on the microscopic structure of the epidermis–dermis layer and the characteristics of blisters on porcine skin, we prove that the porcine skin, instead of the human skin, is feasible as an innovative experimental material for generating friction blisters. Second, the conditions for generating blisters on porcine skin are confirmed using a series of adaptive time-gradient tests. Considering the properties of the censored results, we clarify an inherently safe region in the tangential traction–time relationship, which is based on a nonparametric estimation of the survival function on the subjects. After a condition-matching calculation, this region for the porcine skin is further verified to be consistent with that for the human skin. Third, the safety of the 'stand-up and sit-down' motion of a physical assistant robot user is successfully validated by applying this verification method, which finally proves its practical usability with regard to the possible physical stress hazard.

ARTICLE HISTORY
Received 4 October 2016
Revised 21 January 2017
Accepted 4 April 2017

KEYWORDS
Assistive robotics; human–robot contacting; friction; health and safety; life estimation

1. Introduction

Physical assistant robots, which are directly attached to the human bodies, are expected to provide various opportunities of creating assisting technologies for efficiently transferring power to the human musculoskeletal system [1]. Consequently, physical assistant robots have found increasingly wide applications in various fields [2] from industrial environments [3] to rehabilitation practices [4,5]; however, because of the close human–robot contact, misalignment between the human anatomical joints and the exoskeleton of robot may exert continuous undesired friction force on the human body [6,7], which becomes a potential hazard for the users [8]. Considering the results of the risk assessment, we concentrate on the hazards of friction force, which are unique to the physical assistant robot operation, such as the one caused by anatomical mismatch.

According to ISO 13482 [8], the measurement of hazardous physical stress is required for validating the safety of devices in question for the physical assistant robots, particularly for the restraint type of physical assistant robots. So far, several studies have contributed significantly to the findings for the safety verification of human–robot coexistence systems. Regarding relatively light mechanical impact, Yamada et al. first investigated the limit of human pain tolerance through a biomechanical approach [9,10], and Saito et al. tried to determine the limit by a static measurement [11]. Further, a human–robot contact limit at a whole-body scale was intensively surveyed and provided under static conditions [12], and Haddadin et al. directly related the medical observation of injury to the physical input parameters of the motion of the robot and paved the way for generating safe robot motions with more general terms [13].

Considering the biomechanical aspect, there have not been any reported studies regarding the dependence of tangential component on the harm severity, whereas the hazards of normal force have been considered seriously using the existing safety assessment standard for machinery. However, the friction force exerted by the brace parts of the physical assistant robots can lead to considerably uncomfortable feelings for the users [14]. It has also been observed that the friction force is the main cause of skin friction traumas such as friction blisters and abrasions [15], particularly for patients with poor health condition. In a clinical observation, Okado et al. observed that patients with diabetes or liver cirrhosis obtained friction blister trauma or skin ulcer more easily than

CONTACT Xuewei Mao mao.xuewei@e.mbox.nagoya-u.ac.jp

other users of physical assistant robots [16]. Our study focuses on the grossly neglected friction blister injuries and tries to fill the gap in the existing safety verification methodology by mainly investigating the effect of the friction force on human–robot contact surfaces.

As is evident from some published investigations, the experimental studies of friction blisters have been conducted on living subjects such as humans [17] or animals [18], which inevitably inflict unwanted pain on the subjects [17]. To avoid any possible ethical controversy, Xing et al. employed a dynamic non-linear finite-element model for replicating the blister-characterized structure [19]. Using an algorithm for the outer covering and roof of the blister, the model can qualitatively evaluate the effects of loading environments and contacting materials. In addition, several studies have developed other kinds of simulation models consisting of multiple layers for investigating the relationship among surface treatment, skin condition, and damage caused by friction blisters [20,21]; however, they still contain less detailed information such as the effects of different friction force values on the actual blister generation time and cannot act as a standard for a certain safety validation test. In our study, fresh porcine skin was selected as a novel substitute for living subjects to relieve them from the suffering caused by friction blisters. As validated in previous studies, porcine tissue is a well-suited substitute for human skin [22,23]. Moreover, considering the individualities of experimental subjects, the results obtained using porcine skin can conform better to the results obtained under real human conditions, which differ even in one group of people and are difficult to be simulated using a single fixed model.

From several experimental studies on friction blisters, we can argue that there are several factors affecting the degree of damage caused by friction blisters, such as the loading mode [24], skin surface conditions [15,24], and the individualities of different skin types [15]. A credible safety validation should be conducted under the same condition as that of the target condition [25]. Therefore, the results of the friction blisters obtained from previous tests, which were performed under different environmental conditions, cannot be directly used in our safety verification test, which focuses on a new condition – the utilization of physical assistant robots. During this condition, if the robots are excessively used, the undesired friction force exerted by the robot cuffs may cause blisters on the surface of the human skin contacting with the cuffs. Therefore, experimental results obtained under the condition of rubbing over long periods of time are more practical for our purpose of applying them in the daily use of robots. In addition, considering that the contact state always varies with different ways of using the robots, we selected a rheometer for performing rubbing tests with controlled tangential traction (friction force per unit area) and time. As the tangential traction is unique under different contact states, the experimental condition of a metal head rubbing a piece of porcine skin facilitates the safety verification for various human skin–cuff contact states. Based on this method, the skin damage condition during the utilization of a physical assistant robot can be simulated accurately under the application of repetitive interactive forces between the skin of the user and the cuff of the robot.

In this study, a novel safety verification method is developed for helping the users of physical assistant robots to avoid possible skin friction blisters. This paper is organized as follows: Section 2 provides a description of the entire experimental setup; the section also describes the main processing techniques used for the experimental material before and after the test. In Section 3, the loading principle used in our experiments is first presented, followed by an explanation of the adaptive testing method. Using this specially designed method, the possible blister generation time under a certain tangential traction (friction force per unit area) value can be efficiently confirmed even when there is no obvious macroscopic symptom on the skin surface. Section 4 briefly introduces the preprocessing process for microscopic analysis and then summarizes the unique characteristics of the friction blisters formed on fresh porcine skin, which is based on the observation results. Considering that most of the experimental results obtained from the microscopic observation are censored data, an inherently safe condition region for the tangential traction–time relationship is clarified in this section by conducting a nonparametric estimation of the survival function on the subjects. Furthermore, Section 5 enhances the calculation of the inherently safe threshold to make it more appropriate for the condition of human blister generation. In Section 6, this novel safety verification method is applied to the safety validation of human–robot interaction during a 'stand-up and sit-down' motion, and the feasibility of the method is confirmed by the agreement between our experimental result inferences and microscopic observation results.

2. Experimental material and method

2.1. Experimental material

As a well-suited substitute for human skin, the physiological and biological properties of porcine skin are similar to those of human skin [18], particularly in the epidermis and dermis layers, which are closely related to the generation of friction blisters [15,24]. In the structural aspect, the epidermal thickness of the porcine skin and the ratio of it to the dermal thickness are both similar to those of

the human skin [23,26]. The histological appearance of the porcine skin is demonstrated to be similar to that of the human skin, including the epidermis keratinous protein fractions [27], stratum corneum's variable filament density and areas of cell overlapping [28], and the dermal architecture of collagen fibers and fiber bundles [26], which can significantly affect the friction blister generation. Moreover, it is confirmed that the epidermal–dermal junction of the porcine skin resembles that of the human skin [28]. There are also several studies detailing the similarity of the mechanical properties between human skin and porcine skin, among which, their similarity under dynamic tensile loading helps most in exhibiting the feasibility of porcine skin acting as a substitute for human skin friction blister tests [29]. Therefore, the fresh porcine skin excised from the anterior shank was used as the experimental material. It was delivered to our laboratory within 16 h below a temperature of 4 °C. So as to shape it more similar to human skin, we shaved and cleaned its surface and removed the excessive underneath fat.

2.2. Experimental setup

In most studies about friction blisters [15,30], friction force is regarded as one of the most significant factors for generating blisters. In our experiments, friction force was also selected as the representative direction (tangential direction) of force component, which was applied for emulating the repetitive rubbing motion of the cuff of a physical assistant robot on the skin surface. As the force effects on blisters are also related to the actual contacting area, our study utilized the friction force per unit area as tangential traction. To achieve a horizontal reciprocating rubbing action under controlled tangential traction, the Discovery Hybrid Rheometer (DHR-2-NA, TA Instruments, US) was used for performing oscillating rotational rubbing on the porcine skin with high calibration accuracy (0.1 Pa). During the experiment, the revolving geometry of the DHR acted as a rubbing head and the tangential traction exerted in the skin surface oscillated with a preset frequency and constant amplitude. The normal force was approximately 5 N, and the reason for selecting this value is shown later.

To avoid undesired displacement of the experimental material, a fixation frame was used for clamping the porcine skin on the plate of the rheometer. A sheet of sandpaper (grit size: 40) was attached between the skin and the plate for a firmer fixation, as shown in Figure 1. After every rubbing test, the porcine skin sample was immersed sequentially in 10% formalin solution, 20% sucrose, and 30% sucrose with phosphate-buffered saline for 8 h. Before histological sectioning, the tissue samples

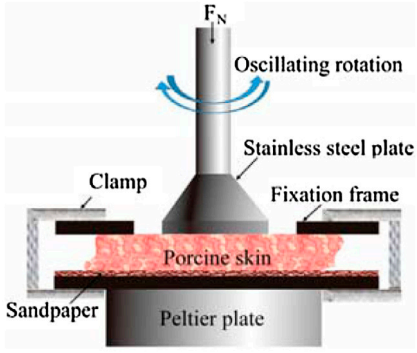

Figure 1. Main experimental apparatus of rubbing test.

were manually cut into fine cubes and mixed with optimal cutting temperature (O.C.T.) compound for fast freezing with dry ice. Subsequently, they were placed in a cryostat (CM 3050 S, Leica Biosystems, Germany) and sectioned at 10 μm after precooling for 30 min. To detect the presence of the skin structure, the histological sections of the samples were stained using the normal H&E staining technique, which stains the basophilic structures in blue using hematoxylin and the acidophilic structures in red using eosin. After dehydration with a descending array of ethanol and xylene, the sections were mounted and observed under a microscope.

As the porcine skin sample after one test was sectioned and examined immediately, every rubbing test needed one new piece of fresh porcine skin, i.e. there were no tested porcine skin samples continuously applied in the subsequent rubbing tests.

3. Experimental design

The distribution of tangential traction on the surface of the skin sample under the rubbing head can be calculated as follows:

$$\tau(r) = \eta\dot{\gamma}(r) = \eta\frac{\Omega r}{H} = \eta\frac{\Omega}{H}\cdot r \tag{1}$$

where η is the viscosity, H is the thickness, and $\dot{\gamma}$ is the shear rate of the porcine skin first confirmed by DHR. Moreover, Ω is the angular velocity measured during the test, and r is the distance from the contact center [31].

Using the contact area between the rubbing head and the tested porcine skin A, the torque of the rubbing head, T, can be calculated as follows:

$$T = \int \mathrm{d}A\cdot\tau(r)\cdot r = \eta\frac{\Omega}{H}\cdot\int r^2\mathrm{d}A \tag{2}$$

As it can also be measured using DHR in real time, the tangential traction distributed on the porcine skin surface can also be calculated as follows:

$$\tau(r) = \frac{2T}{\pi R^4} \cdot r \tag{3}$$

where R is the radius of the contact area.

According to the above equations, we can accurately fix a certain tangential traction value exerted to a target area of the porcine skin surface contacting with the rubbing head of DHR.

With regard to the individuality of porcine skin pieces, it is not sufficiently reliable to conduct only one test for one tangential traction–time point for obtaining the verification data. In addition, as the blister generation cannot be directly observed from the appearance of the skin surface, it is not sufficiently efficient to use the observation of the sections acquiring from a series of fixed time-gradient tests for approaching the possible initial time of blister generation. To solve these two problems, we designed the test method as follows.

First, for one series of experiments under the same tangential traction value, several different rubbing durations were tested with a time gradient of Δt, and for every tangential traction–time condition, one set of tests was conducted with n pieces of porcine skin. Second, under one tangential traction value condition, the rubbing tests were started from a relatively long time. The rubbing time for the next step, T_{k+1}, was decided on the basis of the result of the last step that was obtained using the H&E staining method. Moreover, to avoid the unnecessary tests conducted on areas where no blisters can be generated or all samples can be heavily damaged, it is essential to conduct most of the tests around the condition areas that are worth testing, i.e. under the conditions where about half of the samples can generate blisters, and this area will be investigated in the near future. Therefore, the rubbing time of the next test was decided according to the number of blister samples after the last test, b_k. If most of the samples develop blisters after a test, a shorter rubbing time will be selected for the next step; otherwise, the rubbing time will be increased.

If n is an odd number, T_{k+1} can be calculated as follows:

$$T_{k+1} = \begin{cases} T_k + (\frac{n+1}{2} - b_k)\Delta t & \text{if } b_k < \frac{n+1}{2} \\ T_k + (\frac{n-1}{2} - b_k)\Delta t & \text{otherwise} \end{cases} \tag{4}$$

Similarly, if n is an even number, T_{k+1} can be calculated as follows:

$$T_{k+1} = T_k + \left(\frac{n}{2} - b_k\right)\Delta t \tag{5}$$

As 3 is the smallest number that can help us identify whether a tangential traction–time condition can generate a blister more easily, we fixed n as 3, i.e. three pieces of porcine skin were tested under one tangential traction–rubbing time condition. Moreover, a series of rubbing tests under one tangential traction value was continued until three sets of tests under three different lengths of rubbing time conditions were observed to be ended with three different incidences of blister samples, 33%, 67%, and 100%. Therefore, a series of rubbing tests under one tangential traction value condition contained at least three sets of tests, which rubbed nine pieces of porcine skin under three different time durations of rubbing conditions. In addition, the average value of the previous two rubbing time values might be selected for avoiding the unnecessary repetition test. A more detailed and general experimental procedure flowchart is presented in Appendix 1.

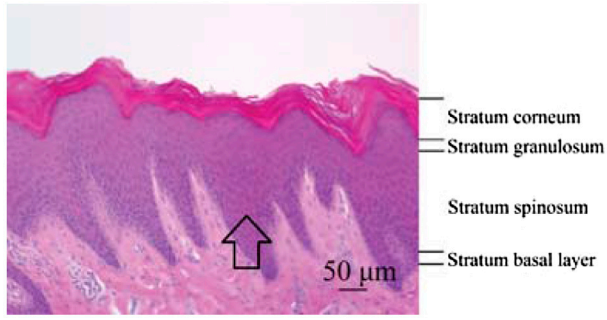

Figure 2. Intact stratum spinosum of porcine skin before tests (indicated by an arrow).

4. Experimental results and discussions

4.1. Feasibility analysis of porcine skin for developing experimental friction blisters

Because of the effect of stress concentration [32], the tangential traction increased sharply when it approached the rim of the surface of the sample, and this part of the skin was typically badly worn. For obtaining relatively stable results, we focused on the condition of the skin located 0.5R from the center of the rubbing area. The appearance of the microscopic porcine skin structure before tests and the appearance of the samples, rubbed under the tangential traction of 32 kPa for 1200 s, are shown in Figures 2 and 3, respectively.

From Figure 2, it can be clearly observed that the skin epidermal structure was maintained intact before the tests. Similar to the human skin [27], the epidermis of the porcine skin also includes the stratum corneum, stratum granulosum, stratum spinosum, and epidermal basal layer. As claimed by the previous studies of experimental friction blisters on human skin [24], the friction force exerted on the skin surface can be transmitted through the stratum corneum and granulosum of the epidermis. Subsequently, the stratum spinosum can be degenerated and some clefts can be produced between the stratum

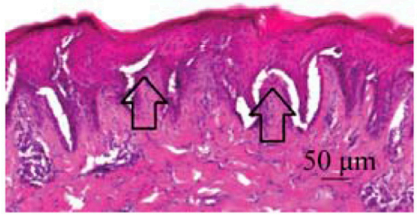

Figure 3. Intra-epidermal clefts of porcine skin after test indicated by arrows.

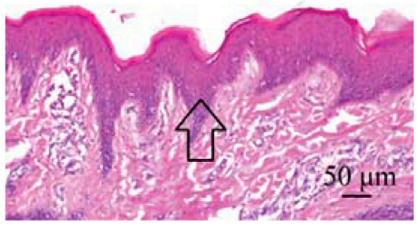

Figure 4. Intact stratum spinosum of porcine skin after test (indicated by arrow).

granulosum and the basal layer. Within a short period of time, those clefts are filled with free fluid from the dermis layer of the skin and macroscopic friction blisters are developed.

Unlike the sample without any rubbing test in Figure 2 and the sample after a shorter rubbing test (900 s) under the same tangential traction in Figure 4, the sample shown in Figure 3 developed severe splits in the stratum spinosum layer. According to the study summarized by Knapik and his colleagues [15], the cavities or clefts of friction blisters produced on human skin are invariably observed at the same intra-epidermal layers, which include the stratum corneum composing the blister roof, the stratum granulosum, and a segment of the stratum spinosum that is traumatically degenerated during the blister generation. As the clefts observed after our rubbing tests were also located in the same intra-epidermal layers and were composed with the intact stratum corneum and stratum granulosum similar to the human friction blisters, we regarded the clefts shown in Figure 3 as an essential evidence of the initial stage of the experimental friction blisters in our tests.

Considering the biophysical property changes in the *in vitro* experiment compared to the *in vivo* experiment, the available fluid left in the skin after excision was insufficient for filling the clefts and raising the blister roof. Therefore, the macroscopic blisters were difficult to be developed on the porcine skin used in our tests. However, those intro-epidermal clefts act well as an indicator of the friction blister generation, which proves that our new experimental model is still effective to be applied to investigate the generation condition of friction blisters.

4.2. Censored properties of current results

After one set of rubbing tests under the same tangential traction–rubbing time condition, the number of pieces of skin that obtained blisters was observed under the microscope. However, the results we observed after rubbing tests were all censored data [33], and it is significantly difficult to obtain the exact time condition of the initial blister generation. For example, if we observe one piece of porcine skin that developed blisters after a rubbing test, then the only information it can provide us is that the blisters were generated before this observation time; however, no one can determine when it was initially generated. Such results are regarded as left-censored data. In contrast, if a piece of skin did not develop blisters after a rubbing test, we can infer that it will develop blisters in the future but we still cannot determine the exact time. Such results are called right-censored data.

We conducted experiments for each set of the porcine skin consisting of three pieces, and the results of all the rubbing tests are summarized with the tangential traction and time as shown in Figure 5. The percentages of generating friction blisters vary: 100%, 67%, and 33%, respectively, from the left to the right in Figure 5.

4.3. Inherently safe thresholds to prevent friction blisters on porcine skin

To estimate the probability of the blister generation on the porcine skin based on the current results, a survival analysis technique for the censored data was selected so that this special state can be taken into consideration [33].

In general, the different groups of the three samples tested under different rubbing time values have similar properties with regard to blister generation. For most of the tangential traction values tested in our experiments, the second piece of porcine skin used less than 50 s for developing blisters after the first piece of skin developed blisters. If we considered the severest state, this piece of skin might develop blisters just after the shortest observation time; i.e. if we did not stop the rubbing test for observation, this piece of skin would develop blisters at the previous stopping time point. As the application of the survival analysis technique requires at least one datum that is not censored, we assumed that only one piece of skin developed blisters exactly at the observation time, instead of one sample developing blisters after this time. Similarly, for almost all the results, the test in which two blisters were generated is only 50 s or

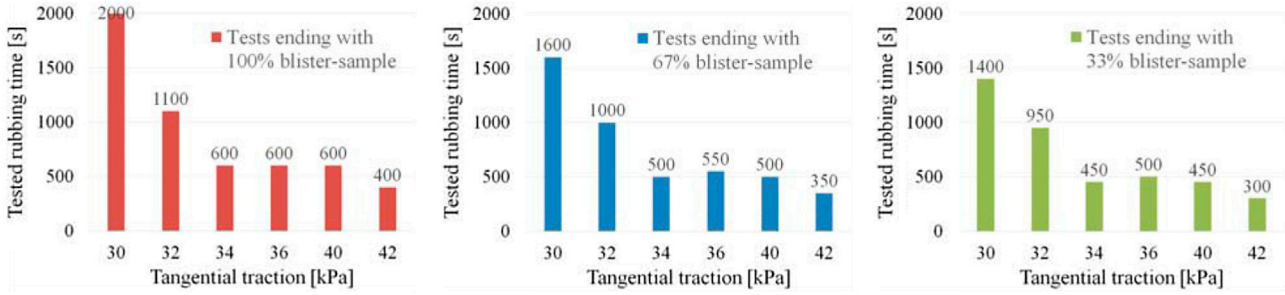

Figure 5. Experimental results after rubbing tests.

100 s shorter than the one in which three blisters were generated under the same tangential traction. Therefore, a similar assumption was considered for the results in which two samples developed blisters; i.e. one more piece of skin developed blisters exactly at the observation time point, instead of one sample developing blisters after this time. According to the above assumptions, the original experimental results can be converted to the ones listed in Table 1.

Under these assumptions, if we consider a grid of time points $0 = t_0 < t_1 < t_2 < \cdots < t_m$ as the rubbing time we tested previously, d_i as the number of samples developing blisters at time t_i, Y_i as the number of samples at risk at time t_i, r_i as the number of samples developing no blisters at time t_i, c_i as the number of samples developing blisters before time t_i, and j as the order of only the time points with left-censored data, then the survival functions for different tangential traction values can be estimated based on the following algorithm [33]:

Step 0: Compute an initial estimate of the survival function, $S_0(t_j)$, at each t_j based on the product-limit estimator while ignoring the left-censored samples,

$$\hat{S}_0(t_j) = \prod_{t_i \le t_j} \left[1 - \frac{d_i}{Y_i}\right] \tag{6}$$

where $i = 1, 2, 3, \ldots; j = 1, 2, 3, \ldots$.

Step (K) - 1: Using the current estimate of the survival function, $S_{K-1}(t_j)$, at each t_j, estimate p_{ji} for $i \le j$:

$$p_{ji} = \frac{S_{K-1}(t_{i-1}) - S_{K-1}(t_i)}{1 - S_{K-1}(t_j)} \tag{7}$$

where $K = 1, 2, 3, \ldots$.

Step (K) - 2: Use p_{ji} for estimating the number of samples developing blisters at time t_i:

$$\hat{d}_i = d_i + \sum_{j=1}^{m} c_j p_{ji} \tag{8}$$

where m is the total number of left-censored samples.

Step (K) - 3: Calculate the usual product-limit estimator based on $\hat{d}_i$ and r_i at t_i, while ignoring the left-censored samples. If this estimate, $S_K(t)$, is close to $S_{K-1}(t)$ for all t_i, stop this procedure; if not, increase K by 1 and go back to Step (K) - 1 and repeat the subsequent steps.

Based on the $\hat{S}(t)$ estimated above, the mean time for the blister generation restricted to the interval $[0, \tau]$, where τ is the time required for obtaining three blister samples, can be estimated using

$$\hat{\mu}_\tau = \int_0^\tau \hat{S}(t)\mathrm{d}t \tag{9}$$

The expected value of the deviation of the blister generation probability, $\hat{\sigma}$, can also be computed using

$$\hat{\sigma}_\tau = \sqrt{\sum_{i=1}^{n} p_i \cdot (t_i - \hat{\mu}_\tau)^2} \tag{10}$$

where $p_i = 1 - S_i - \sum_{k=0}^{i-1} p_k$, $p_0 = 0$ and $i = 1, 2, 3, \ldots$.

Combining the estimated mean value and variance of the blister generation time condition, a time point for every tangential traction value, such as $\hat{\mu}_\tau - 3\hat{\sigma}_\tau$, can be calculated with a relatively less blister generation probability. This kind of points is defined as the inherently safe tangential traction–time conditions in this paper, and the practical method of defining inherently safe conditions for the usage of robots is discussed in the later part.

To provide robot users with more options, three kinds of inherently safe time conditions indicating three different levels of safety are computed by $\hat{\mu}_\tau - 2\hat{\sigma}_\tau$, $\hat{\mu}_\tau - 3\hat{\sigma}_\tau$ and $\hat{\mu}_\tau - 4\hat{\sigma}_\tau$, and summarized in Table 2. The inherently safe points and all the time points tested under one tangential traction value, 30 kPa, are shown in Figure 6, from which, it can be deduced that the possibility of obtaining blisters under the inherently safe condition is effectively reduced.

Three regression curves were drawn from the three types of inherently safe time points. They were regarded

Table 1. Converted experimental results based on assumptions.

Group of tested samples	Incidence of samples/ Survival times [s]	Tangential traction [kPa] 42	40	36	34	32	30
1st 3 of 9 samples	33%	(0, 300)	(0, 450)	(0, 500)	(0, 450)	(0, 950)	(0, 1400)
	33%	300	450	500	450	950	1400
	33%	[300, +∞)	[450, +∞)	[500, +∞)	[450, +∞)	[950, +∞)	[1400, +∞)
2nd 3 of 9 samples	67%	(0, 350)	(0, 500)	(0, 550)	(0, 500)	(0, 1000)	(0, 1600)
	33%	350	500	550	500	1000	1600
3rd 3 of 9 samples	0%	[350, +∞)	[500, +∞)	[550, +∞)	[500, +∞)	[1000, +∞)	[1600, +∞)
	100%	(0, 400)	(0, 600)	(0, 600)	(0, 600)	(0, 1100)	(0, 2000)

Table 2. Inherently safe conditions to prevent friction blisters on porcine skin.

Tangential traction [*kPa*]	τ [s]	$\hat{\mu}_\tau$ [s]	$\hat{\sigma}_\tau$ [s]	$\hat{\mu}_\tau - 2\hat{\sigma}_\tau$ [s]	$\hat{\mu}_\tau - 3\hat{\sigma}_\tau$ [s]	$\hat{\mu}_\tau - 4\hat{\sigma}_\tau$ [s]
42	400	322.92	24.91	273.1	248.19	223.28
40	600	472.92	24.91	423.1	398.19	373.28
36	600	522.92	24.91	473.1	448.19	423.28
34	600	472.92	24.91	423.1	398.19	373.28
32	1100	972.92	24.91	923.1	898.19	873.28
30	2000	1491.66	99.65	1292.36	1192.71	1093.06

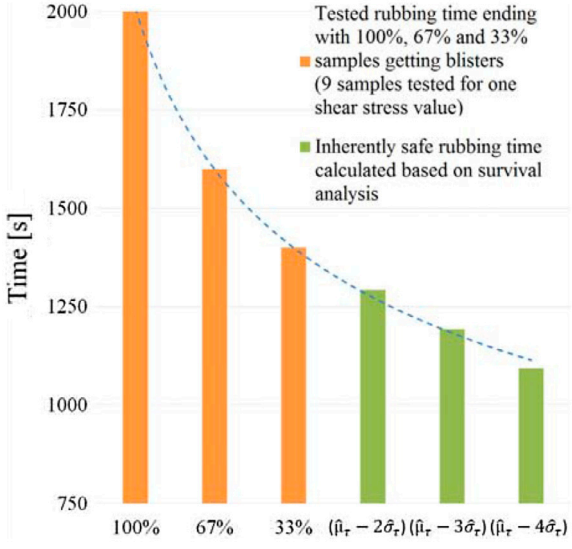

Figure 6. Comparison between the inherently safe time condition and tested time condition.

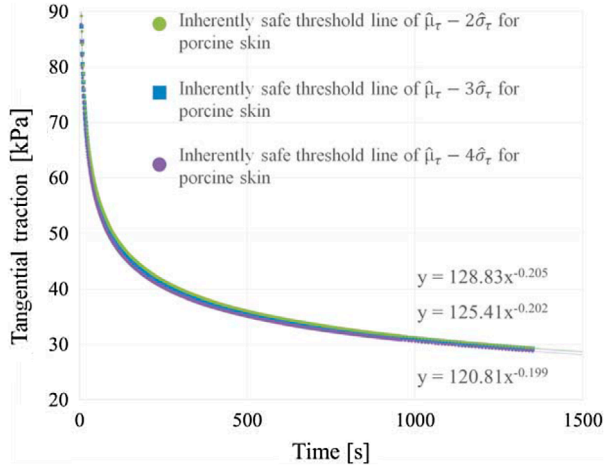

Figure 7. Inherently safe condition to prevent friction blisters on porcine skin.

as three types of inherently safe thresholds for exhibiting a unique characteristic of the porcine skin friction blisters in the tangential traction–time relationship (Figure 7). Moreover, the equations of these thresholds are shown in the same figure, where the vertical axis, y, represents the tangential traction condition and the horizontal axis, x, represents the time condition. It should be noted that the three inherently safe thresholds shown in Figure 7 only act as an example for three possible types of the inherently safe conditions. The inherently safe conditions with the type of $\hat{\mu}_\tau - \alpha\hat{\sigma}_\tau$ can help the users of robots to avoid friction blisters; however, the real number α should be decided according to the various specific social backgrounds.

5. Feasibility confirmation of porcine skin for safety verification

To confirm the feasibility of using porcine skin as an experimental model for developing friction blisters, the characteristics of blister generation should match with the characteristics obtained by the studies conducted on

normal human skin, such as the one performed by Naylor [24]. The normal force set in Naylor's study was also 5 N [24], and the tested area on the human body was also similar to our tested area; therefore, it is possible for us to combine the results of human skin tests with ours. However, in our rubbing tests, the tangential traction was set as the parameter for analyzing the interaction between the rubbing head and the porcine skin surface, which was different from Naylor's results described with the compression and average friction force only [24]. To compare the blister generation characteristics, a condition-matching calculation was applied for converting the parameters used in the Naylor's study to ours.

5.1. Matching different experimental criteria

As Naylor applied a small hemisphere head for rubbing [34], the tangential traction value tested in their studies can be approximately calculated based on the Amontons' law [32]

$$q(r) = \frac{3\mu_d P}{2\pi a^2}\frac{\sqrt{a^2 - r^2}}{a} \tag{11}$$

where μ_d is the dynamic friction coefficient between the human skin and the rubbing head, P is the total load compressing the skin surface, and a is the radius of the contact circle. According to Hertz theory [32], a can be calculated as follows:

$$a = \left(\frac{3PR}{4E^*}\right)^{\frac{1}{3}} \tag{12}$$

where R is the relative curvatures. The principal curvature of the two surfaces contacting with each other, R_1 and R_2, are used for calculating R with the following equation.

$$\frac{1}{R} = \frac{1}{R_1} + \frac{1}{R_2} \tag{13}$$

In addition, using the elastic moduli of the two surfaces contacting with each other, E_1 and E_2, and Poisson's ratios, ν_1 and ν_2, E^* can be calculated as follows:

$$\frac{1}{E^*} = \frac{1-\nu_1^2}{E_1} + \frac{1-\nu_2^2}{E_2} \tag{14}$$

The rubbing head used in the Naylor's study was fabricated using polythene. As its elastic modulus is considerably larger than that of the skin, we can ignore its contribution to E^*. With regard to the tested human skin area, which was located in about the middle third of the anterior surface of the tibia [24], the Poisson's ratio and the elastic modulus used in the above equations were assumed to be 0.45 and 130 kPa, respectively, [35]. Based on this condition-matching calculation, the friction blister generation conditions tested in the Naylor's study can be finally described with the rubbing time and its corresponding tangential traction values. Moreover, as the highest tangential traction in the center of the contacting circle played a dominant role in generating blisters, the *p(0)* was considered as a representative value in the tangential direction.

5.2. Feasibility analysis of porcine skin for safety verification test

To provide a more appropriate inherently safe threshold for human blister generation state, we calculated the inherently safe points from the Naylor's results [24] and used them as a reference for improving the previous threshold. As the tangential traction gradient in our study is 2 kPa, the tangential traction values tested in the Naylor's study were also separated into several groups with a difference of 2 kPa. The subjects tested in one group were regarded as being tested under the medial tangential traction of this group, and then, their inherently safe points, $\hat{\mu}_\tau - 2\hat{\sigma}_\tau$, $\hat{\mu}_\tau - 3\hat{\sigma}_\tau$, and $\hat{\mu}_\tau - 4\hat{\sigma}_\tau$, were computed using the similar method described in Section 4.3. The results of this calculation are summarized in Table B1 of Appendix 2.

As the negative values in Table B1 had no practical significance, these negative values were ignored. Only the positive values were added to the inherently safe points obtained in Section 4.3 for calculating an enhanced inherently safe threshold. In addition, the inherently safe points calculated using the excessively concentrated data (with $\hat{\sigma}_\tau < 5$) were also removed from this enhanced operation because they contributed less to the statistical distribution. As the tangential traction applied on the skin of the users of the robots is usually not significantly large, this time we only focused on the area of lower tangential traction. The three enhanced inherently safe thresholds are shown in Figure 8. From Figure 8, it can be concluded that the three different thresholds are almost similar to each other.

Therefore, the medial threshold calculated according to the inherently safe points of $\hat{\mu}_\tau - 3\hat{\sigma}_\tau$ was selected as an example of the inherently safe threshold and used in the following discussion. As noted before, the real number α in $\hat{\mu}_\tau - \alpha\hat{\sigma}_\tau$ should be selected adequately in the community where the safety verification data are used considering other factors such as social background.

To confirm the differences between the enhanced threshold and the previous one, we combined the curves for these two thresholds in Figure 9. As shown in the figure, the inherently safe points calculated using part of

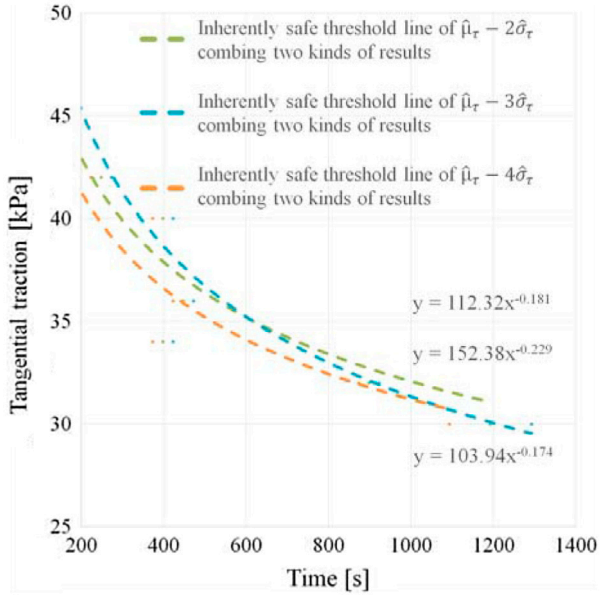

Figure 8. Inherently safe threshold improved by combining porcine skin's and human skin's test results.

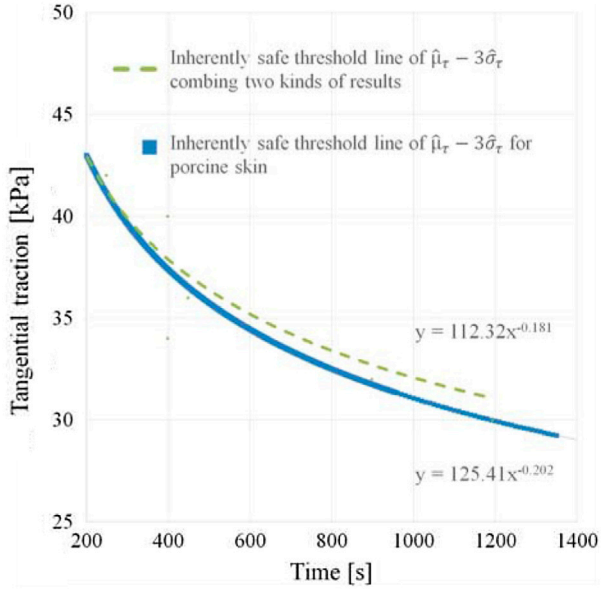

Figure 9. Comparison of two kinds of inherently safe thresholds.

the human test results do not change the entire threshold considerably. The agreement between these two thresholds again proves that it is feasible to apply our novel method for determining the inherently safe threshold for human users.

5.3. Analysis of influence of outlier on final result

Considering that our study mainly focuses on the practical operation of physical assistant robots, a more detailed discussion is essential for the points in the relatively

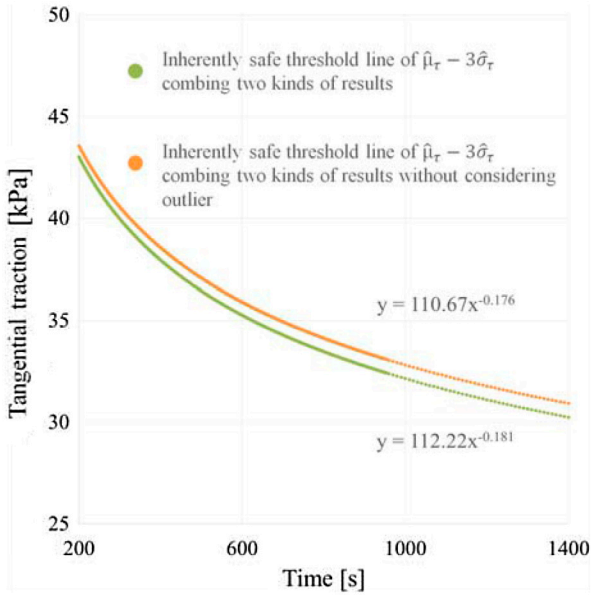

Figure 10. Comparison of different thresholds for analyzing outlier's influence.

longtime region in Figure 9. After the regression curve was drawn from the inherently safe points and was regarded as the inherently safe threshold, one point (398.19 s–34 kPa) constituting a small inconsistency with this curve, in the long time, was observed.

For analyzing the influence of this outlier on the entire threshold, a new inherently safe threshold was calculated from the same group of safe points but ignored the outlier point. The new threshold was compared with the previous one, and the combined threshold curves are shown in Figure 10. As 1600 s was the longest rubbing time under which at least one no-blister result can still be acquired, more attention was paid to the time interval that is appropriately 1600 s; however, there was only a small difference, 0.68 kPa at maximum, between these two thresholds, and the percentage of this difference to the entire corresponding tangential traction range was only 2%. Therefore, the influence of the outlier is regarded to be sufficiently small and can be eliminated. Moreover, the new threshold computed without the outlier is applied to the final safety verification.

6. Safety validation test using porcine skin and manipulator

Owing to the difference in the contact states between the stainless steel plate–porcine skin in Figure 1 and the cuff–human skin of the physical assistant robot, it is essential to confirm the feasibility of the characteristics obtained in Section 5. Two series of safety validation tests were performed. These tests focused on the 'stand-up and sit-down' motion of a human subject, which had the ability to exhibit a general function of a physical assistant robot.

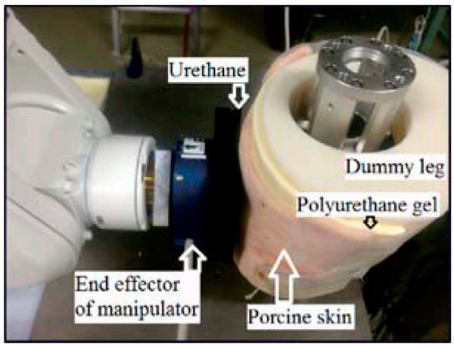

Figure 11. Experimental setup of preliminary application.

6.1. Experimental design of safety validation

6.1.1. For original 'stand-up and sit-down' motion

In our previous studies [36], the original cuff–skin interactive force was firstly measured on human subjects wearing physical assistant robots. After equipping a contact sensing function by implementing iterative feedback tuning (IFT) control, a manipulator exerted the interactive force repetitively on a piece of dummy skin using a cuff mounted on its end tip [36]. This manipulator was also utilized for performing our safety validation tests. Moreover, in the first series of the validation tests, the manipulator rubbed the porcine skin by repeating the actual human skin–robot interactive force, which was measured during the 'stand-up and sit-down' motion of a human subject, on the skin surface.

6.1.2. For relatively higher human–robot interactive force

Considering the hazards of the relatively higher part in the entire human–robot interactive force, it is essential to ensure the feasibility of our safety verification method under higher friction force. Therefore, the original human–robot interactive force was increased by 1.3 times, and a 2.5 s part with the highest force value in the middle was repeated on porcine skin in the second series of safety validation tests.

6.2. Experimental setup of safety validation

Figure 11 shows the main part of the experimental apparatus used in the validation test, where the cuff of a physical assistant robot is simulated using a piece of urethane foam and the structure of fat and muscle are simulated by pasting the polyurethane gel (whose hardness, as measured using the ASKER Durometer Type C, is 0) on the dummy leg. The porcine skin was finally pasted on the gel after the same preprocessing method described in Section 2.1 and the multiple-layer structure was fixed using tapes and bands.

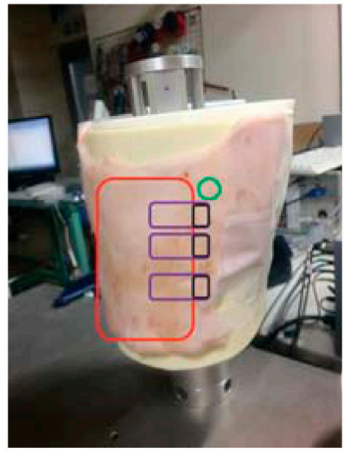

Figure 12. Samples' positions for safety validation.

6.3. Experimental result inferences

6.3.1. For original 'stand-up and sit-down' motion

In the first series of validation tests, three pieces of intact porcine skin were tested under the same interactive force as the one measured during the 'stand-up and sit-down' motion of a robot user. According to previous studies of the normal rehabilitation training program, patients usually need 100 repetitions at most for enhancing their 'stand-up and sit-down' motion every day [37,38]. To conduct sufficiently long and convincing tests, each of the test lasted for 1800 s. Moreover, the human–robot interactive force of one 'stand-up and sit-down' motion was repeated for more than 200 times.

As the smallest contact area between the porcine skin and the cuff was approximately 12×10^{-4} m^2 and the highest friction force exerted on the porcine skin was 27.7 N, the highest tangential traction exerted on the porcine skin was approximately 23 kPa. As shown in Figure 10, the experimental condition, 1800 s–23 kPa, is located in the inherently safe region and the tested skin should be relatively safe in less than 7500 s. Even if the highest tangential traction is exerted on the porcine skin for the entire 1800 s, there should be few blisters observed in the skin samples. Therefore, we supposed that the porcine skin would remain intact after the rubbing test.

6.3.2. For relatively higher part of human–robot interactive force

After the original force value was increased by 1.3 times, the highest tangential traction exerted on the porcine skin became 30 kPa. As shown in Figure 10, the experimental condition, 1800 s–30 kPa, is located in the hazardous region and there may be friction blisters generated in the tested porcine skin. Two other durations, 1000 s and 2600 s, were also considered for confirming the feasibility of our safety verification method under different conditions, which should, respectively, acquire intact porcine

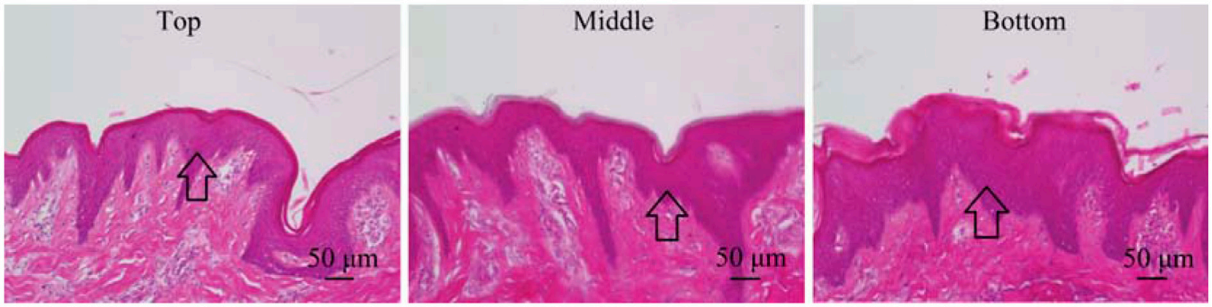

Figure 13. Appearances of three porcine skin samples after first series of safe validation tests (arrows indicate intact stratum spinosum).

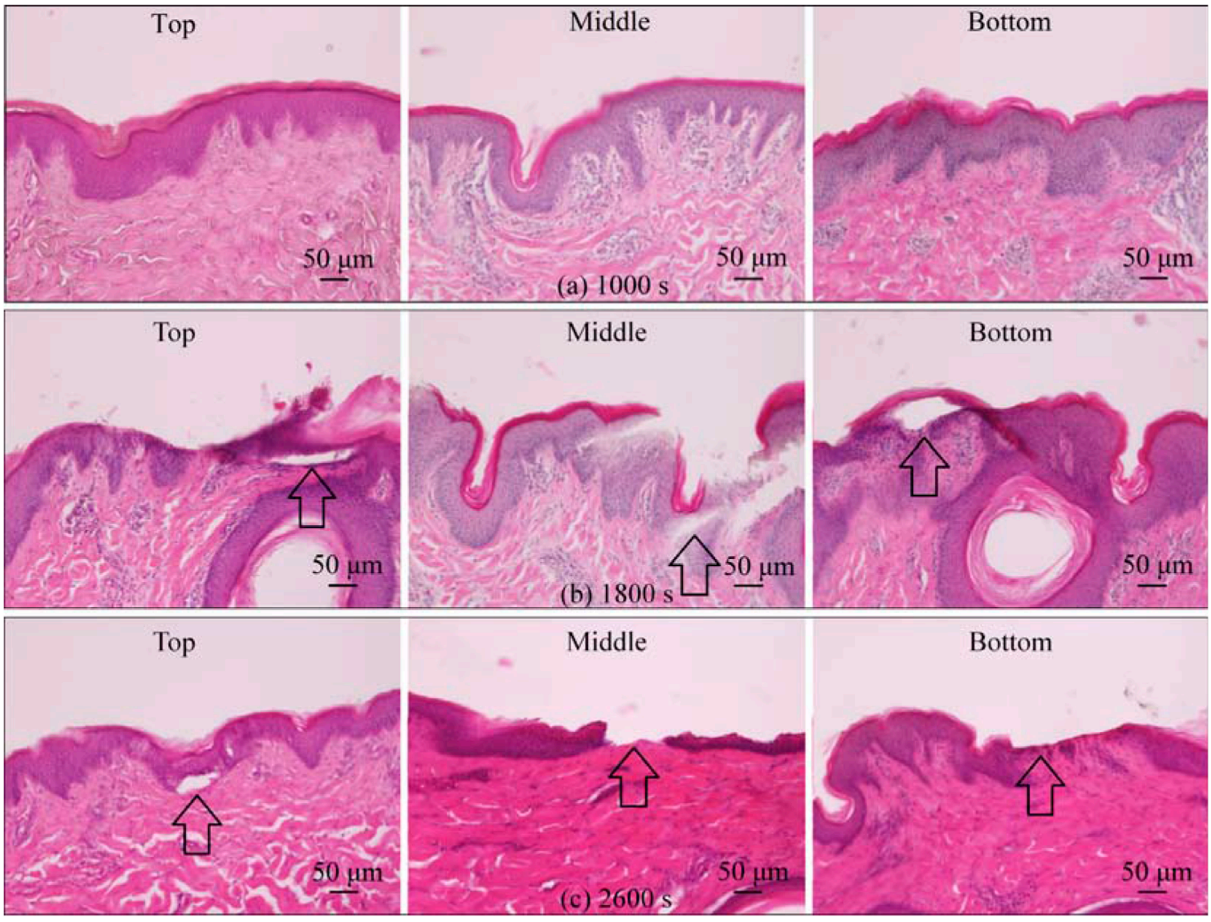

Figure 14. Appearances of nine porcine skin samples after second series of safe validation tests (arrows indicate friction blisters or damaged skin surface).

skin and damaged samples according to our verification results in Figure 10.

6.4. Safety validation test results

The positions of samples used for observation after the tests are shown in Figure 12. The area of the porcine skin surface under rubbing is indicated by a red rectangle in Figure 12. Three samples were considered, each from the top, medium, and bottom parts of the skin–cuff contact area after every validation test. The purple rectangles show the examined areas. Each of them contains a small additional control part, which did not contact the cuff during the entire test. Moreover, the part, which is located far from the skin–cuff contact area and marked by a green circle shown in Figure 12, was considered for providing a control sample and for ensuring the intact condition of the original skin.

6.4.1. For original 'stand-up and sit-down' motion

Using the same method described in Sections 2.1 and 4, the porcine skin samples after validation tests were processed and examined. After the first series of tests, no blister was observed in the skin samples. As shown in Figure 13, the appearances of the skin samples selected from three positions are almost similar to each other, with a slight stratum corneum avulsion but an intact stratum spinosum. This result indicates that the duration time of 1800 s 'stand-up and sit-down' motion is sufficiently short for the users of the robot system with the cuff under our experiments to accept it.

6.4.2. For relatively higher part of human–robot interactive force

The results of the second series of safety validation tests are shown in Figure 14. From Figure 14(a), it can be clearly observed that the porcine skin samples after the 1000 s test still maintain intact epidermis layers, without considering from where the sample is selected. However, several friction blisters can be observed in the epidermis layer from 1800 s as indicated by the arrows in Figure 14(b). After 2600 s tests, the epidermis layers of the tested samples were heavily damaged or even removed from the skin surface as shown in Figure 14(c).

The second series of safety validation tests effectively demonstrates that the inherently safe condition summarized using our verification method described in Section 5 is sufficiently feasible for helping the robot users to avoid blister injuries, even though the experimental environment in the verification method is different from the environment of the actual robot usage. Moreover, all these safety validation test results are consistent with our inference for relatively longer time of rubbing tests, which cannot be evidently concluded from the Naylor's study. The validation tests confirm not only the feasibility of our novel safety verification method for the actual human–robot contact state, but also its practicability for the relatively longtime utilization of physical assistant robots.

7. Conclusions

A novel safety verification method was established in this study for preventing friction traumas on the skin of physical assistant robot users. To the best of our knowledge, we first confirmed the feasibility of using porcine skin as a substitute material for the experimental friction blister generation by performing a series of time-gradient rubbing tests. We also identified its unique properties with reference to previous results for human skin. In addition, we used an adaptive repetitive testing method for efficiently clarifying the blister generation condition while considering the subject individualities. An inherently safe condition region for the tangential traction–time relationship was then estimated by a nonparametric survival analysis technique, which efficiently used the experimental results containing the censored data. After performing a condition-matching calculation, it was observed that the inherently safe condition for the porcine skin was similar to that for the human skin. This finding further verified the feasibility of our novel safety verification method for the human users. Our novel method was then used for performing safety validation tests focusing on the 'stand-up and sit-down' motion of a physical assistant robot user. Based on the safety verification results, correct inferences were made for the experimental results, which confirmed that our novel method is sufficiently practical for the safety validation of the physical assistant robots with possible physical stress hazards.

Considering that the daily usage of a physical assistant robot typically exerts relatively low tangential traction on the skin of the users, in this study, we provide more attention to the low tangential traction area. In the future, more tests will be performed on porcine skin at higher tangential traction values for further enhancing the inherently safe threshold.

Acknowledgements

The authors would also like to thank Dr. Cota Nabeshima, Cyberdyne Inc., for discussing the possible injury in the framework of contact safety associated with physical assistant robots. The authors are also grateful to Prof. Susumu Hara, Nagoya University, for his helpful advice of data analysis improvement, and Mr. Ishiguro Kenji, Nagoya University, for his technical support for human–robot data collection.

Disclosure statement

No potential conflict of interest was reported by the authors.

Funding

This work was supported by NEDO (New Energy and Industrial Technology Development Organization) and AMED (Japan Agency for Medical Research and Development) [grant number 16he1202004h0004].

Notes on contributors

Xuewei Mao received the BE and MS degree in Measurement and Control Technology and Instrument in 2010 and 2013, respectively, from the Graduate School of Precision Instrument and Opto-electronics Engineering, Tianjin University, China. Since 2013, she has been a PhD candidate at Nagoya University, Japan. Her main areas of research interests are mechanical safety and human-robot interaction.

Yoji Yamada received a doctor degree from Tokyo Institute of Technology in 1990. He had been with Toyota Technological Institute, Nagoya, Japan, since 1983 and became an associate professor in the Graduate School of the Institute. In 2004, he joined Intelligent Systems Research Institute of National Institute of Advanced Industrial and Science Technology (AIST). In 2008, he moved to the Department of Mechanical Science and Engineering, Graduate School of Engineering, Nagoya University as a professor. He is a member of Robotics Society of Japan, and his current research interests include safety and intelligence technology in human/machine systems, their robotic sensing and control.

Yasuhiro Akiyama received the BE degree in Engineering from Tokyo Institute of Technology, Tokyo, Japan, in 2006, and the MS and the PhD degree in Engineering from the University of Tokyo, Tokyo, Japan, in 2008 and 2011, respectively. Since 2016, he has been an assistant professor at the Graduate School of Engineering, Nagoya University, Japan. His main areas of research interests are mechanical safety, humanrobot interaction, and manned space mission.

Shogo Okamoto received MS and PhD degrees in Information Sciences in 2007 and 2010, respectively, from the Graduate School of Information Sciences, Tohoku University. Since 2016, he has been an associate professor at the Graduate School of Engineering, Nagoya University. His research interests include haptics and human-assistive technology.

Kengo Yoshida received the BE and MS degree in Mechano-informatics and Systems in 2013 and 2015, respectively, from Nagoya University, Nagoya, Japan.

ORCID

Xuewei Mao http://orcid.org/0000-0002-2300-5723

References

[1] Rosen J, Brand M, Fuchs MB, et al. A myosignal-based powered exoskeleton system. IEEE Trans Syst Man Cybern part A: Syst Hum. 2001;31(3):210–222.
[2] Pons JL. Wearable robots: biomechatronic exoskeletons. Hoboken (NJ): Wiley; 2008.
[3] Naito J, Obinata G, Nakayama A, et al. Development of a wearable robot for assisting carpentry workers. Intern J Adv Robot Syst. 2007;4(4):431–436.
[4] Hornby TG, Zemon DH, Campbell D. Robotic-assisted, body-weight-supported treadmill training in individuals following motor incomplete spinal cord injury. Phys Ther. 2005;85(1):52–66.
[5] Wier LM, Hatcher MS, Lo AC. Effect of robot-assisted versus conventional body-weight-supported treadmill training on quality of life for people with multiple sclerosis. J Rehabil Res Dev. 2011;48(4):483.
[6] Akiyama Y, Yamada Y, Okamoto S. Interaction forces beneath cuffs of physical assistant robots and their motion-based estimation. Adv Robot. 2015;29(20):1315–1329.
[7] Zanotto D, Akiyama Y, Stegall P, et al. Knee joint misalignment in exoskeletons for the lower extremities: Effects on user's gait. IEEE Trans Robot. 2015;31(4):978–987.
[8] International Standards Organization (ISO). Robots and robotics devices - safety requirements for personal care robot. Geneva: ISO; 2014. Standard No. ISO 13482: 2014.
[9] Yamada Y, Suita K, Ikeda H, et al. Evaluation of pain tolerance based on a biomechanical method for human-robot coexistence. Trans Jpn Soc Mech Eng. 1997;63:2814–1819. Japanese.
[10] Yamada Y, Hirasawa Y, Huang S, et al. Human-robot contact in the safeguarding space. IEEE/ASME Trans Mechatron. 1997;2(4):230–236.
[11] Saito T, Ikeda T. Measuring system and analytical method of pain tolerance to mechanical stimulus for sale design of human-collaborative robots. Specif Res Rep Natl Inst Ind Saf. 2005;33:15–23.
[12] ISO. Robots and robotic devices - safety requirements for industrial robots - collaborative operation. Geneva: ISO; 2013. Standard No. ISO/CDTS 15066.
[13] Haddadin S, Haddadin S, Khoury A, et al. On making robots understand safety: Embedding injury knowledge into control. Int J Robot Res. 2012;31(13):1578–1602.
[14] Schmalz T, Knopf E, Drewitz H, et al. Analysis of biomechanical effectiveness of valgus-inducing knee brace for osteoarthritis of knee. J Rehabil Res Dev. 2010;47(5):419–430.
[15] Knapik JJ, Reynolds KL, Duplantis KL, et al. Friction blisters. Sports Med. 1995;20(3):136–147.
[16] Kyouko O. Current status of the introduction of lower extremity functional training with the robot suit HAL in our hospital. Jpn J Press Ulcers. 2014;16(3):289. Japanese.
[17] Hashmi F, Richards BS, Forghany S, et al. The formation of friction blisters on the foot: the development of a laboratory-based blister creation model. Skin Res Technol. 2013;19(1):e479–e489.
[18] Goldstein B, Sanders J. Skin response to repetitive mechanical stress: a new experimental model in pig. Arch Phys Med Rehabil. 1998;79(3):265–272.
[19] Xing M, Pan N, Zhong W, et al. Skin friction blistering: computer model. Skin Res Technol. 2007;13(3):310–316.
[20] Guerra C, Schwartz C. Investigation of the influence of textiles and surface treatments on blistering using a novel simulant. Skin Res Technol. 2012;18(1):94–100.
[21] Guerra C, Schwartz C. Development of a synthetic skin simulant platform for the investigation of dermal blistering mechanics. Tribol Lett. 2011;44(2):223–228.
[22] Meyer W. [comments on the suitability of swine skin as a biological model for human skin]. Der Hautarzt; Zeitschrift fur Dermatologie, Venerologie, und verwandte Gebiete. 1996;47(3):178–182. German.
[23] Swindle M. Porcine integumentary system models: part 1-dermal toxicology. Sinclair Res. 2008. [cited 2016 Dec 10]; [7p.]. Available from:http://www.sinclairresearch.com/assets/Porcine-Integumentary-System-Model-Part-1.locked.pdf.
[24] Naylor P. Experimental friction blisters. Br J Dermatol. 1955;67(10):327–342.
[25] Akiyama Y, Okamoto S, Yamada Y, et al. Measurement of contact behavior including slippage of cuff when using wearable physical assistant robot. IEEE Trans Neural Syst Rehabil Eng. 2016;24:784–793.
[26] Vardaxis NJ, Brans TA, Boon ME, et al. Confocal laser scanning microscopy of porcine skin: implications for

human wound healing studies. J Anat. 1997;190(04): 601–611.
[27] Sullivan TP, Eaglstein WH, Davis SC, et al. The pig as a model for human wound healing. Wound Repair Regen. 2001;9(2):66–76.
[28] Monteiro-Riviere N. Ultrastructural evaluation of the porcine integument. New York (NY): Plenum Press; 1986.
[29] Lim J, Hong J, Chen WW, et al. Mechanical response of pig skin under dynamic tensile loading. Int J Impact Eng. 2011;38(2):130–135.
[30] Hoffman MD. Etiological foundation for practical strategies to prevent exercise-related foot blisters. Curr Sports Med Rep. 2016;15(5):330–335.
[31] Hetnarski RB, Ignaczak J. Mathematical theory of elasticity. Boca Raton (Florida): CRC Press; 2004.
[32] Johnson KL, Johnson KL. Contact mechanics. New York (NY): Cambridge University Press; 1987.
[33] Klein JP, Moeschberger ML. Survival analysis: techniques for censored and truncated data. New York (NY): Springer; 2003.
[34] Naylor P. The skin surface and friction. Br J Dermatol. 1955;67(7):239–248.
[35] Mak AF, Liu GH, Lee S. Biomechanical assessment of below-knee residual limb tissue. J Rehabil Res Dev. 1994;31(3):188–198.
[36] Yoshida K, Yamada Y, Akiyama Y, et al. 20th robotics symposia, Nagano, Japan; 2015 Mar 15–16.
[37] Monger C, Carr JH, Fowler V. Evaluation of a home-based exercise and training programme to improve sit-to-stand in patients with chronic stroke. Clin Rehabil. 2002;16(4):361–367.
[38] Canning CG, Shepherd RB, Carr JH, et al. A randomized controlled trial of the effects of intensive sit-to-stand training after recent traumatic brain injury on sit-to-stand performance. Clin Rehabil. 2003;17(4):355–362.

Appendix 1

This appendix provides a more detailed and general introduction to the experimental procedure presented in Section 3. The main experimental parameters and experimental procedure flowchart are listed in Table A1 and shown in Figure A1, respectively, where T_{bn} and b_k are initially set as 0.

Table A1. Main parameters of improved experimental method.

k	order of test
T_k	rubbing duration for kth test
T_{bn}	rubbing duration developing blisters in n samples
b_k	number of samples with blisters generated obtained in kth test
Δt	gradient of time
T_{esti}	estimation of initial time when blister is generated
Q	$Q = \prod_{i=1}^{k}(b_i - 1) + \prod_{i=1}^{k}(b_i - 2) + \prod_{i=1}^{k}(b_i - 3)$

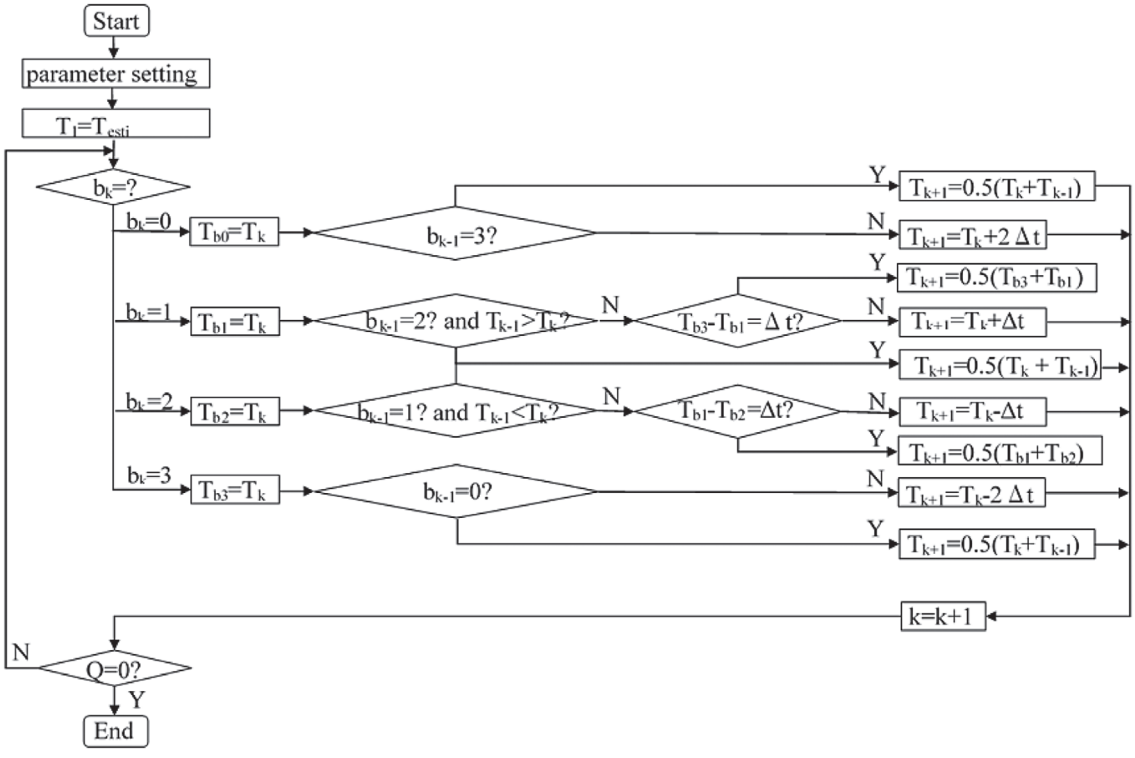

Figure A1. Experimental procedure flow chart.

Appendix 2

The inherently safe points for human skin tested in Naylor's study [24] were computed using the similar method described in Section 4.3. The results of this calculation are summarized in Table B1.

Table B1. Inherently safe conditions against friction blister generation on human skin.

Tangential traction [*kPa*]	τ [s]	$\hat{\mu}_\tau$ [s]	$\hat{\sigma}_\tau$ [s]	$\hat{\mu}_\tau - 2\hat{\sigma}_\tau$ [s]	$\hat{\mu}_\tau - 3\hat{\sigma}_\tau$ [s]	$\hat{\mu}_\tau - 4\hat{\sigma}_\tau$ [s]
78	102	96	4.9	86.2	81.3	76.4
75	76	75.5	0.5	74.5	74	73.5
73	108	87	20.05	46.9	26.85	6.8
71	123	88.5	34.5	19.5	-15	-49.5
69	165	111.43	25.78	59.87	34.09	8.31
67	153	118.2	25.29	67.62	42.33	17.04
65	192	129.86	37.08	55.7	18.62	-18.46
63	195	128.32	38.91	50.5	11.59	-27.32
61	237	145.5	52.09	41.32	-10.77	-62.86
59	294	153.73	57.80	38.13	-19.67	-77.47
57	255	159	48.73	61.54	12.81	-35.92
55	264	217.8	56.01	105.78	49.77	-6.24
53	354	227.57	78.16	71.25	-6.91	-85.07
51	414	264.75	96.24	72.27	-23.97	-120.21